Paleoceanography and Paleoclimatology

Key Points:
- Concurrent Antarctic ice sheet growth and CO_2 level rise can occur because of disequilibrium between ice volume and climate
- The disequilibrium and CO_2-ice volume phase differences grow with increasing frequency of the forcing
- Larger amplitude CO_2 variability causes larger amplitude ice volume variability and a smaller average ice sheet

Correspondence to:
L. B. Stap,
lennert.stap@awi.de

Anti-Phased Miocene Ice Volume and CO₂ Changes by Transient Antarctic Ice Sheet Variability

L. B. Stap[1] [ID], **G. Knorr[1]** [ID], and **G. Lohmann[1]** [ID]

[1]Alfred-Wegener-Institut, Helmholtz-Zentrum für Polar-und Meeresforschung, Bremerhaven, Germany

Abstract Geological evidence indicates large continental-scale Antarctic ice volume variations during the early and mid-Miocene. On million-year timescales, these variations can largely be explained by equilibrium Antarctic ice sheet (AIS) simulations. In contrast, on shorter orbital timescales, the AIS needs not be in equilibrium with the forcing and ice volume variations may be substantially different. Here, we introduce a conceptual model, based on ice dynamical model results, to investigate the difference between transient variability and equilibrium differences of the Miocene AIS. In our model, an ice sheet will grow (shrink) by a specific rate when it is smaller (larger) than its equilibrium size. We show that phases of concurrent ice volume increase and rising CO_2 levels are possible, even though the equilibrium ice volume decreases monotonically with CO_2. When the AIS volume is out of equilibrium with the forcing climate, the ice sheet can still be adapting to a relatively large equilibrium size, although CO_2 is rising after a phase of decrease. A delayed response of Antarctic ice volume to (covarying) solar insolation and CO_2 concentrations can cause discrepancies between Miocene solar insolation and benthic $\delta^{18}O$ variability. Increasing forcing frequency leads to a larger disequilibrium and consequently larger CO_2-ice volume phase differences. Furthermore, an amplified forcing amplitude causes larger amplitude ice volume variability, because the growth and decay rates depend on the forcing. It also leads to a reduced average ice volume, resulting from the growth rates generally being smaller than the decay rates.

Plain Language Summary The early and mid-Miocene (23–14 Myr ago) was the last period in Earth's history when the Antarctic ice sheet (AIS) size changed between being almost completely vanished and its current magnitude. So far, ice modelers have tried explaining this large-scale AIS variability using steady-state experiments, in which the final ice volume is in equilibrium with the forcing climate. In these simulations, phases of simultaneous ice sheet growth and CO_2 increase have to be caused by increased precipitation outweighing increased melt in a warmer climate. Conversely, simultaneous ice sheet decay and CO_2 decrease must be due to decreased precipitation exceeding decreased melt. Here, we provide an alternative explanation for these phases, based on the notion that the slowly evolving AIS is not in equilibrium with the forcing climate. In our model, an ice sheet will grow (shrink) by a specific rate when it is smaller (larger) than its equilibrium size. The AIS can then still be adapting to a relatively large equilibrium size, when CO_2 is already increasing again after an initial drop. It can also continue decaying after a reversal from rising to sinking CO_2 levels. Our results serve to aid the interpretation of Miocene geological oxygen isotope data.

1. Introduction

The early and mid-Miocene (23 to 14 Myr ago) is an essential period for studying the dynamics of the Antarctic ice sheet (AIS) in a warmer climate, since it was the last period in Earth's history when extensive continental-scale (tens of meters sea level equivalent) AIS changes occurred. Indeed, geological evidence from sea level records (John et al., 2011; Kominz et al., 2008; Miller et al., 2005) and ice-proximal ocean sediment cores (e.g., Levy et al., 2016) indicates that the AIS ranged from being almost vanished to its modern-day marine-terminating configuration during this time. Moreover, benthic $\delta^{18}O$ records show large fluctuations on shorter, predominantly orbital timescales (e.g., Cramer et al., 2009; De Vleeschouwer et al., 2017; Holbourn et al., 2013; Liebrand et al., 2011, 2017; Levy et al., 2019; Zachos et al., 2008). However, different factors cause significant uncertainty in the interpretation of these benthic $\delta^{18}O$ fluctuations.

One factor was the focus of an earlier study (Stap et al., 2019). It concerns to what extent these benthic $\delta^{18}O$ fluctuations are caused by deep-sea temperature changes and to what extent by ice volume changes
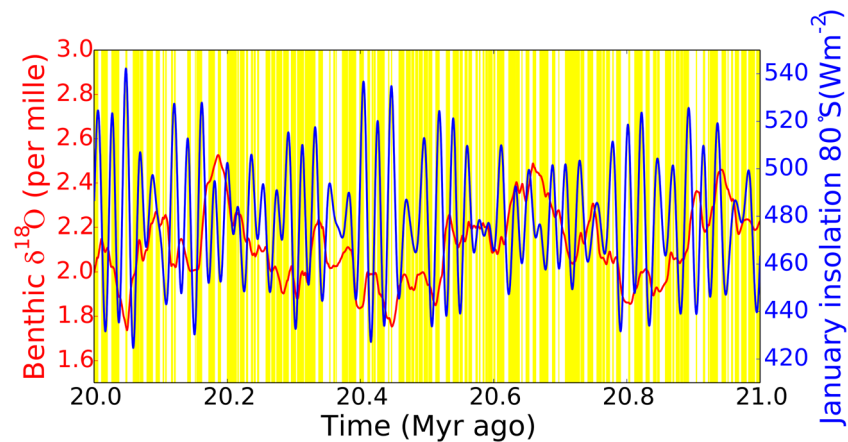
Figure 1. An 80°S January mean insolation from Laskar et al. (2004) (blue) and the stacked benthic $\delta^{18}O$ record of Zachos et al. (2008) interpolated to 100 years (red), over the period 21 to 20 Myr ago. Discrepancies between insolation and benthic $\delta^{18}O$, that is, times when both simultaneously increase or decrease, are marked yellow.

(e.g., Bijl et al., 2018; Billups & Schrag, 2002; Holbourn et al., 2013; Langebroek et al., 2010; Lear et al., 2010; Liebrand et al., 2011, 2017; Shevenell et al., 2008). Note that ice volume changes mainly originate from the AIS as land ice cover on the Northern Hemisphere was probably only limited at the time (Maslin et al., 1998). On the basis of equilibrium simulations, AIS modeling studies have demonstrated the importance of including Antarctic bedrock topography changes (Colleoni et al., 2018) and ice sheet-climate feedbacks, ice calving parameterizations, and changes in the ice sheet's oxygen isotopic composition (Gasson et al., 2016), for simulating strong ice sheet-induced benthic $\delta^{18}O$ variations. However, we found that the slow response time of the AIS to orbital timescale forcing changes significantly reduces the magnitude of ice volume variability and hence its contribution to benthic $\delta^{18}O$ fluctuations, in transient simulations (Stap et al., 2019).

Here, we consider another factor causing uncertainty, which concerns the phase relation between Miocene benthic $\delta^{18}O$ fluctuations and solar insolation forcing changes caused by orbital variations (Laskar et al., 2004). We expect an anti-phase relation between the effect of orbital variations on Southern Hemisphere summer insolation and Antarctic ice volume. Ignoring the potentially considerable influence of deep-sea temperature changes (e.g., Hartman et al., 2018; Hutchinson et al., 2019; Stap et al., 2019), this would be reflected in an anti-phase relation between Southern Hemisphere insolation and benthic $\delta^{18}O$. In Figure 1, we show that for the stacked record of Zachos et al. (2008), this not always the case during the period 21 to 20 Myr ago. Although their duration depends on the age model used, such anti-phased fluctuations of benthic $\delta^{18}O$ and Southern Hemisphere insolation are a robust feature in different global benthic $\delta^{18}O$ records throughout the early and mid-Miocene (Cramer et al., 2009; De Vleeschouwer et al., 2017; Zachos et al., 2008). A fundamental consequence of equilibrium simulations is that simultaneous growth of ice volume and CO_2 level or solar insolation increase has to be caused by a larger increase in accumulation than in ablation due to the induced warmer temperatures (Oerlemans, 1991). When this is not the case, assuming equilibrium, discrepancies between solar insolation and benthic $\delta^{18}O$ variations can only be explained as a consequence of counterbalancing insolation and CO_2 effects on temperature due to anti-phased changes. As an alternative explanation, we here explore discrepancies between solar insolation and benthic $\delta^{18}O$ variability arising from disequilibrium between transient covarying insolation and CO_2 changes and ice volume changes. We take this disequilibrium perspective to study the relation between atmospheric CO_2 and ice volume and consequently the transient variability of the Miocene AIS, by using a conceptual model.

In previous research, conceptual models have been used to investigate transient ice volume variability during the Pleistocene, which was mainly constituted by the waxing and waning of large ice sheets on the North American and Eurasian continents (e.g., Calder, 1974; Huybers, 2009; Huybers & Wunsch, 2005; Imbrie & Imbrie, 1980; Parrenin & Paillard, 2003). These models contained a difference in timescale between growth and decay of ice sheets, based on physical knowledge from early dynamical ice sheet modeling (Weertman, 1964). Growth and decay rates were fixed (Huybers & Wunsch, 2005; Imbrie & Imbrie, 1980), stochastic (Huybers & Wunsch, 2005), or depending, for example, on the existing ice volume (Huybers,

2009; Parrenin & Paillard, 2003). Criteria based on "control" parameters, mostly orbital parameters regulating solar insolation, were used to determine whether an ice sheet is in growth or in decay phase. These criteria were typically tuned to match ice sheet volumes with benthic $\delta^{18}O$ data.

Here, our aim is to analyze the difference in tendency between the transient ice volume variability and equilibrium differences, due to CO_2-driven climate change. In principle, this is possible using any conceptual model with a stable equilibrium solution and a finite response scale. However, we introduce a similar model to address this difference more directly. Our model is based on the notion that an ice sheet will grow when it is smaller and shrink when it is larger, than its explicitly prescribed equilibrium size.

First, we analyze a simple linear relation between the control parameter (C) and equilibrium ice volume with specified growth and decay rates. We investigate the influence on transient ice volume variability of the relationship between the change rate of the equilibrium ice volume and these growth and decay rates. In particular, we focus on the possibility of ice sheet growth during times of rising C, even though the equilibrium ice volume decreases monotonically with C. Furthermore, we analyze the sensitivity of ice volume variability to the amplitude and frequency of the forcing variability. Thereafter, we apply our model to the Miocene AIS, using an input CO_2-equilibrium ice volume relation derived from results of the 3D thermodynamical ice sheet model—the Parallel Ice Sheet Model (PISM) (Stap et al., 2019). By using these results, we circumvent the aforementioned problem that the precise influence of ice volume and deep-sea temperature changes on Miocene $\delta^{18}O$ variations is still highly uncertain. We match our conceptual growth and decay rates to transient PISM results. Based on these rates, we explain the occurrence of phases of concurrent AIS growth (decay) and CO_2 level rise (fall), as well as the dependence of the duration of these phases on the forcing frequency. Furthermore, we predict the influence of reducing the amplitude of CO_2 variability on mean ice volume and ice volume variability. Lastly, we discuss the implications of our results, by analyzing simulations over the period 21 to 20 Myr ago forced by CO_2 variability based on Southern Hemisphere summer insolation. We show how, in absence of other effects, the delayed and nonlinear response of Antarctic ice volume to (covarying) solar insolation and CO_2 concentrations alone can cause discrepancies between solar insolation and benthic $\delta^{18}O$ variability during the Miocene.

2. Model and Methods

In this study, we employ a conceptual model of transient ice volume variability. It is based on the notion that at any level of a control parameter, which can for instance be CO_2 or temperature, an ice sheet will grow or shrink toward an equilibrium state. In our model, the control parameter-equilibrium ice volume (C-V_{eq}) relation of the ice sheet, as well as the growth and decay rates, have to be prescribed. The C-V_{eq} relation can contain hysteresis, so that it has a top branch and a bottom branch. If the ice volume (V) is smaller than the specified bottom branch equilibrium solution (V_{eq_bot}) for the applied value of the control parameter (C) at a time step, the ice volume increases by the growth rate (g). Oppositely, it decreases by the decay rate (d) when it is larger than the top branch equilibrium solution (V_{eq_top}). The growth and decay rates can be constant but may also depend on the control parameter, the ice volume, and the difference between the ice volume and the equilibrium ice volume. If V is in between the top and bottom branch solutions, it is not clear what would happen to an ice sheet in reality. In our model, by default, the volume is kept unchanged in this case, but we discuss the influence of this choice on our results.

$$\text{If } V < V_{eq\_bot}(C) : \frac{dV(t)}{dt} = g \tag{1}$$

$$\text{If } V > V_{eq\_top}(C) : \frac{dV(t)}{dt} = d \tag{2}$$

$$\text{Else } : \frac{dV(t)}{dt} = 0 \tag{3}$$

3. Results

3.1. The Difference Between Transient Ice Volume Variability and Equilibrium Differences

To explore the difference between transient ice volume variability and equilibrium differences, we first prescribe a simple linear C-V_{eq} relation without any hysteresis: $V_{eq\_bot} = V_{eq\_top} = 1 - C$ (Figure 2a). All variables
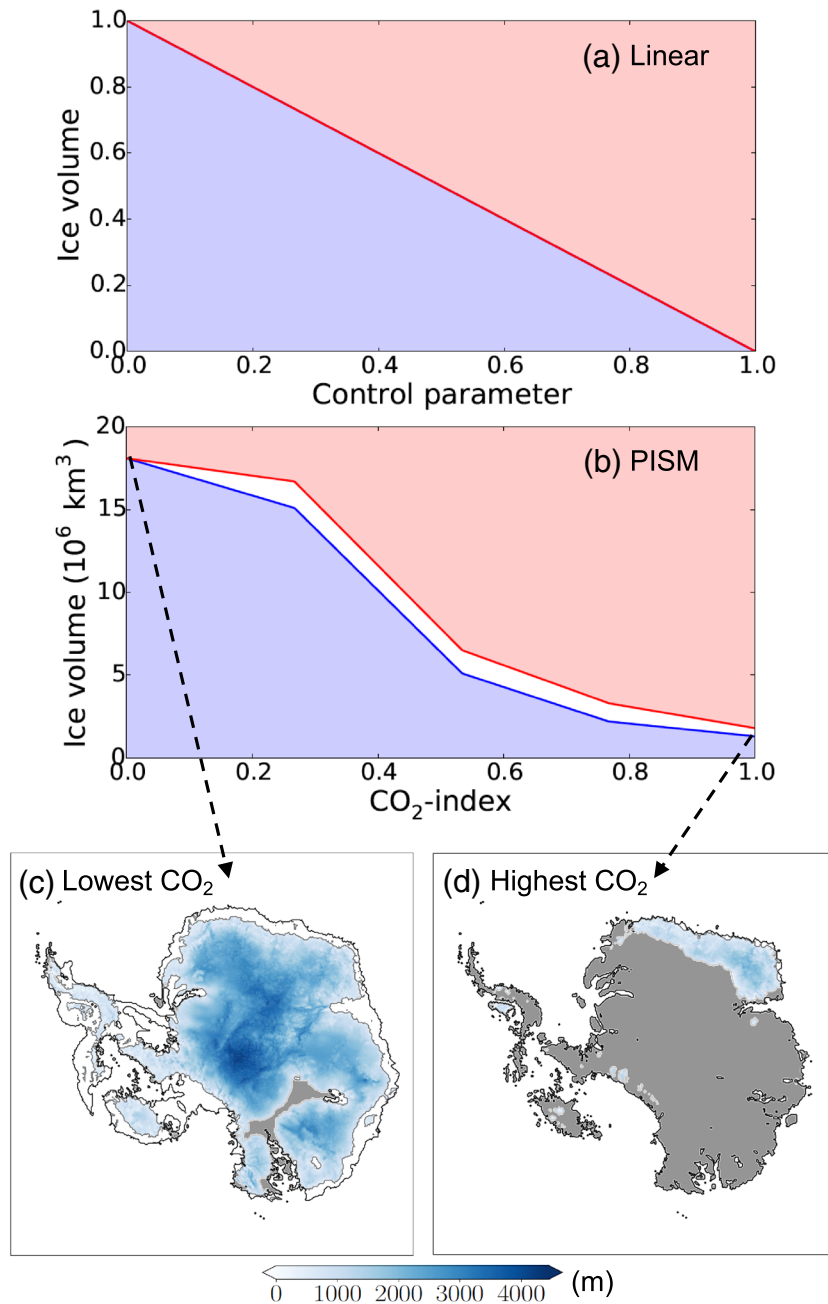
Figure 2. (a) Bottom branch (blue line) and top branch (red line) of the simple linear C-V_{eq} relation without hysteresis (bottom branch and top branch overlap) and (b) of the CO_2-index-V_{eq} relation based on PISM results (Table 2), used as input for the conceptual model. The blue shaded area marks where the ice sheet is smaller than equilibrium and the red shaded area where it is larger. (c) Ice thickness from steady-state simulations of the Miocene Antarctic ice sheet using PISM (Stap et al., 2019), started with a present-day topography (Bedmap2) after deglaciation and isostatic rebound, for the lowest CO_2 level and (d) for the highest CO_2 level. Intermediate level results are not shown here. The gray line indicates the edge of the grounded ice sheet, the black line shows the edge of the continent or ice shelf, and gray areas indicate land that is not glaciated.

Table 1
Conceptual Model Experiments Performed Using a Simple Linear C-V_{eq} Relation

Name	Forcing amplitude	Growth rate	Decay rate	Duration of forcing cycle
$g_{0.01}d_{0.01}$	1 (0 to 1)	0.01	0.01	200 time steps
$g_{0.004}d_{0.004}$	1 (0 to 1)	0.004	0.004	200 time steps
$g_{0.004}d_{0.004}$_slow	1 (0 to 1)	0.004	0.004	400 time steps
$g_{0.002}d_{0.004}$	1 (0 to 1)	0.002	0.004	200 time steps
$g_{0.002}d_{0.004}$_half	0.5 (0.25 to 0.75)	0.002	0.004	200 time steps
$g_{nc}d_{nc}$	1 (0 to 1)	$0.006 \times (V_{eq} - V)$	$0.012 \times (V - V_{eq})$	200 time steps
$g_{nc}d_{nc}$_half	0.5 (0.25 to 0.75)	$0.006 \times (V_{eq} - V)$	$0.012 \times (V - V_{eq})$	200 time steps

Note. Five forcing cycles are performed per experiment.

are unitless. We linearly change the control parameter (C) from 1 to 0 to 1 with a period of 200 time steps and run the model for 1,000 time steps (Table 1; Figure 3a, gray). Initial ice volume is zero.

If we set both the growth and the decay rate equal to the equilibrium change rate ($g_{0.01}d_{0.01}$), the ice sheets remain in equilibrium throughout the run and the ice volume simply follows C (not shown). When the growth and decay rates are reduced ($g_{0.004}d_{0.004}$), however, the ice sheet is smaller than equilibrium at the lowest level of C (Figure 3, green solid lines). It continues to grow when C is increased again, to the
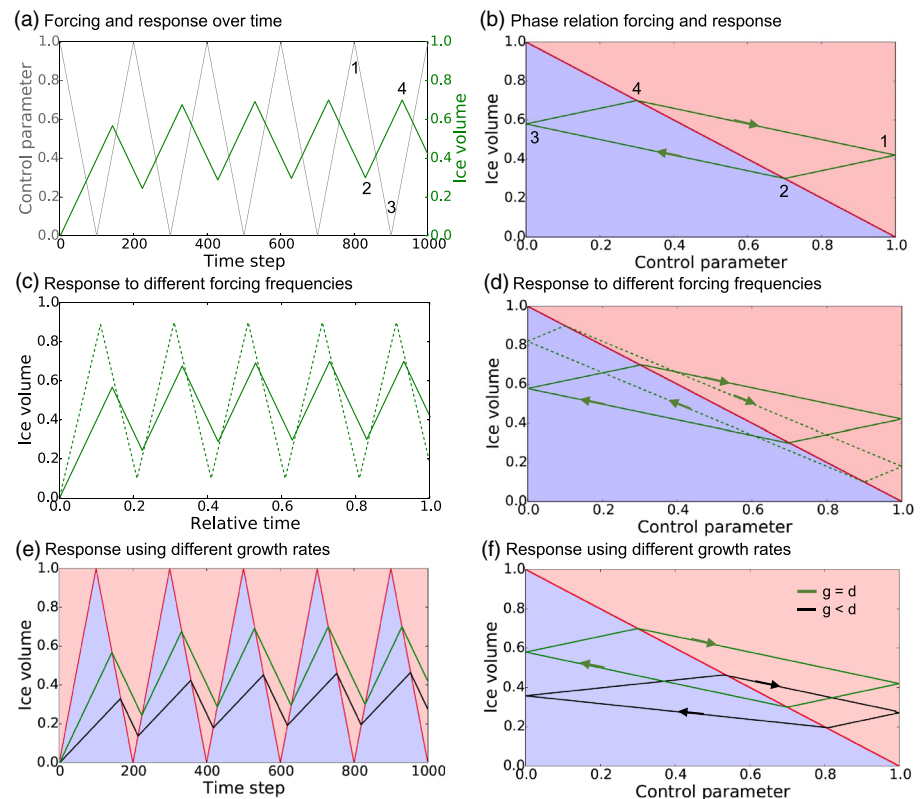

Figure 3. Results of the conceptual model using the simple linear C-V_{eq} relation (Figure 2a). (a) Evolution of the control parameter (gray) and ice volume over time and (b) equilibrium-cycle relation between the control parameter and ice volume (arrows show the progression direction), for experiment $g_{0.004}d_{0.004}$ (green solid). Numbers indicate the equilibrium cycle: (1) forcing starts to decrease, (2) ice volume attains minimum, (3) forcing starts to increase, and (4) ice volume attains maximum. (c, d) Similar for experiments $g_{0.004}d_{0.004}$ (green solid) and $g_{0.004}d_{0.004}$_slow (green dashed) (in panel c, no forcing is shown, and relative time with respect to the total simulation length is shown rather than absolute time). (e, f) Similar for experiments $g_{0.004}d_{0.004}$ (green) and $g_{0.002}d_{0.004}$ (black) (in panel e, absolute time is shown). The blue and red lines show the progression of the bottom and top branch equilibrium ice volumes, respectively.
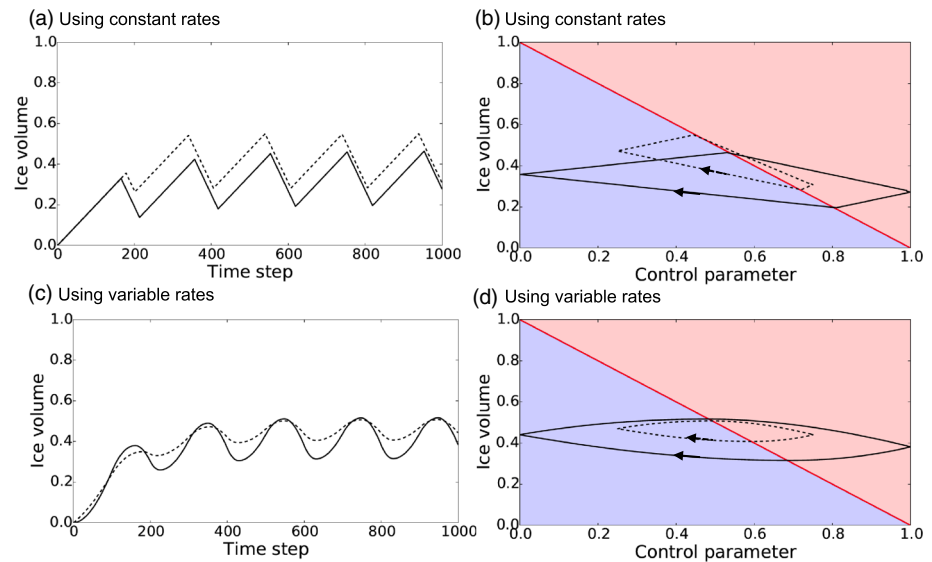
Figure 4. Results of the conceptual model using the simple linear C-V_{eq} relation. (a) Evolution of ice volume over time and (b) equilibrium-cycle relation between the control parameter and ice volume, for experiments $g_{0.002}d_{0.004}$ (solid) and $g_{0.002}d_{0.004}$_half (dashed). (c, d) Similar for experiments $g_{nc}d_{nc}$ (solid) and $g_{nc}d_{nc}$_half (dashed).

point where equilibrium is reached. Likewise, the ice sheet continues to shrink after a reversal from an increasing to a decreasing C. Hence, phase differences between ice volume and the forcing are introduced. Furthermore, the amplitude of ice volume variability increases with decreasing forcing frequency ($g_{0.004}d_{0.004}$_slow; Figures 3c and 3d, green dashed lines). This can be attributed to the fact that the ice sheet has a longer time to build up and decay, which means a larger ice body can wax and wane. In case of lower forcing frequency, the ice sheet remains closer to its equilibrium size. The ice sheet then attains its equilibrium size relatively faster after a reversal of the forcing change. Therefore, the periods of concurrent ice volume increase and CO_2 rise and ice volume decrease and CO_2 decline are relatively shorter.

In the equilibrium cycle of simulation $g_{0.004}d_{0.004}$, the growth and decay phases of ice volume take an equal amount of time. When we implement a growth rate that is smaller than the decay rate ($g_{0.002}d_{0.004}$), however, the growth phase lasts longer than the decay phase in the equilibrium cycle, even though the forcing cycle is still symmetrical (Figures 3e and 3f, black lines). This constitutes a sawtooth pattern in the evolution of ice volume over time. The duration of the phases is determined by the ratio between the growth and decay rates and the amplitude of ice volume variability by their absolute magnitudes. Decreasing the growth rate prolongs the growth phase and reduces ice volume variability. Increasing the decay rate also prolongs the growth phase but increases ice volume variability.

A 50% reduction of forcing variability amplitude ($g_{0.002}d_{0.004}$_half) leads to an increase of the mean ice volume but does not affect the variability (Figures 4a and 4b). When the growth and decay rates depend on the difference between the ice volume and the equilibrium ice volume ($g_{nc}d_{nc}$ and $g_{nc}d_{nc}$_half), however, we obtain reduced amplitude ice volume variability with smaller forcing amplitude (Figures 4c and 4d). A reduction of the forcing amplitude leads to smaller differences between the ice volume and the equilibrium ice volume. This now causes smaller growth and decay rates and consequently smaller amplitude ice volume variability.

In the analysis so far, we have considered a simple linear C-V_{eq} relation without any hysteresis. In Appendix A, we show that most of our results remain qualitatively unchanged when we use a C-V_{eq} relation with appreciable hysteresis. This holds true for different ways of handling the situation when an ice sheet has a volume in between the bottom and top branch equilibrium ice volume (i.e., letting the ice volume grow, keeping it unchanged, and letting it decay). It is important to note, however, that when the ice sheet is kept unchanged between the bottom and top branches (our default option), a reduction of the forcing variability amplitude leads to smaller ice volume variability even in the case of constant growth and decay rates for the C-V_{eq} relation with hysteresis.

Table 2
Results of the Equilibrium Experiments at Different CO_2 Levels for the Miocene Antarctic Ice Sheet, Performed Using PISM (Stap et al., 2019)

	CO_2 index	Ice volume (10^6 km^3)
Bottom branch	1	1.3
	0.7671	2.2
	0.5342	5.1
	0.2671	15.1
	0	18.1
Top branch	0.2671	16.7
	0.5342	6.5
	0.7671	3.3
	1	1.8

Note. In this study, these ice volumes are used to construct an CO_2-index-V_{eq} relation serving as input for the conceptual model (Figure 2b).

3.2. Application to the Miocene AIS

3.2.1. CO_2-Index-V_{eq} Relation

To apply our conceptual model to the Miocene AIS, we prescribe a C-V_{eq} (in this case CO_2-index-V_{eq}) relation based on ice dynamical model results we presented in an earlier study (Stap et al., 2019) (Figures 2c and 2d). These were obtained by running the 3D thermodynamical PISM version 0.7.3 (Bueler & Brown, 2009; Winkelmann et al., 2011) into equilibrium using Miocene forcing conditions (precipitation, near-surface atmospheric, and 3D ocean temperatures). PISM uses a combination of the shallow ice approximation (SIA) and shallow shelf approximation (SSA) to solve the grounded ice velocities and only the SSA for the floating ice velocities. The surface mass balance is calculated using a positive degree day scheme and subshelf melt using a quadratic temperature relation. The forcing conditions were taken from Stärz et al. (2017), who simulated the early and mid-Miocene climate using the coupled atmosphere-ocean general circulation model (GCM) COSMOS (Jungclaus et al., 2006) under three CO_2 levels (278, 450, and 600 ppm). As detailed in Stap et al. (2019), we refer to the CO_2 levels in a relative (low, medium, and high) rather than absolute sense. While retaining the shape, this serves to eliminate model and model setup dependency of the absolute values of the CO_2-ice volume relation from our results. Anomalies of the COSMOS simulations with respect to a preindustrial control run were added to a base climate provided by the 1970–2000 average of ERA-40 reanalysis data (Uppala et al., 2005) and the 1955–2006 average of the World Ocean Database 2009 data set (Locarnini et al., 2010). PISM simulations were conducted using climate forcing with low (CO_2-index $i = 0$), medium ($i = 0.5342$), and high ($i = 1$) CO_2 levels. Additional simulations were performed using forcing conditions in between the low and medium ($i = 0.2671$) and medium and high ($i = 0.7671$) CO_2 levels, by taking the average of the two enclosing climates. The simulations were started without any ice, and with Antarctic bedrock topography taken from the Bedmap2 reconstruction (Fretwell et al., 2013), isostatically rebounded after removal of the ice. We supplement these simulations here by previously unpublished PISM runs under the same climate forcing conditions, but started from ice and Antarctic bedrock topography conditions taken from the results of the low-CO_2 PISM simulation, to complete the hysteresis loop (Table 2). In order to construct a continuous CO_2-index-V_{eq} relation, we assume that the equilibrium ice volume varies linearly between these equilibrated states (Figure 2b).

3.2.2. Growth and Decay Rates

Using time steps of 100 years, we repeat the transient simulations of Stap et al. (2019) with the conceptual model using the same CO_2-index to interpolate between the forcing climates. The index is linearly changed with time from 1 to 0 to 1, with periods of 100, 400, and 40 kyr and the conceptual model integration time is adapted to the forcing period and set to 100, 400, and 200 kyr. The growth and decay rates are then calibrated to find a reasonably close correspondence between the transient conceptual model simulations and the PISM simulations of Stap et al. (2019):
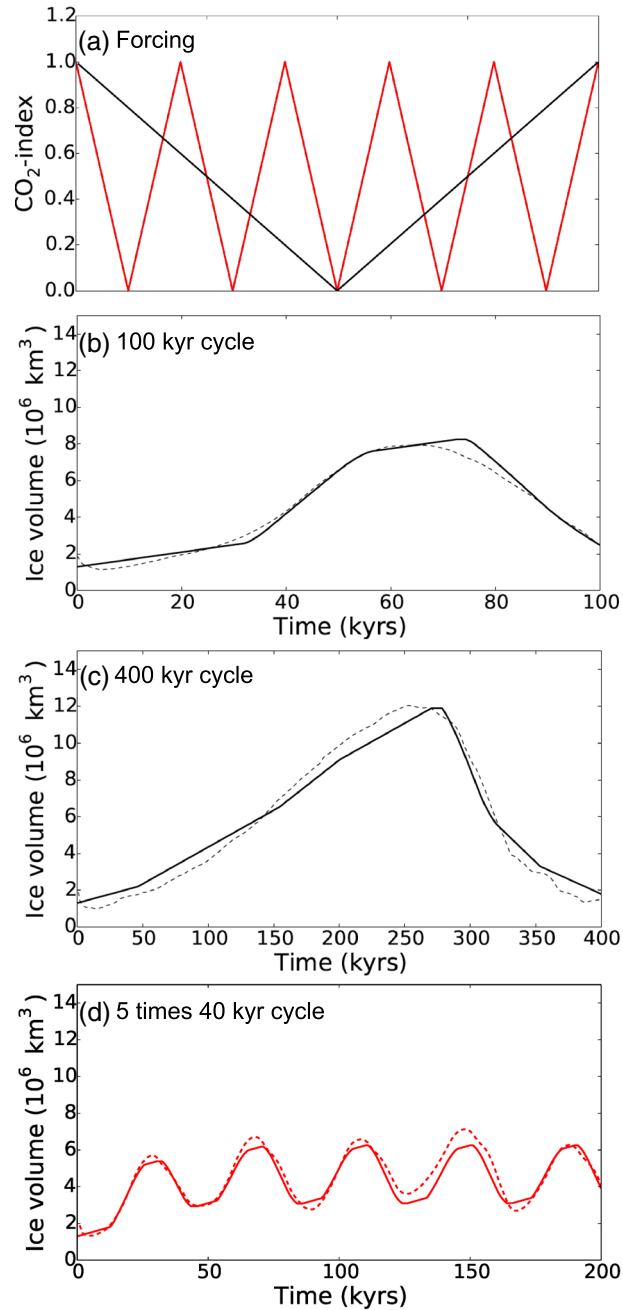
Figure 5. Forcing and results of the transient simulations that are used as a tuning target for the growth and decay rates of the conceptual model. (a) The forcing CO_2-index is linearly changed over time from 1 to 0, and back to 1, over the course of 100 kyr, and 400 kyr (black), and five times over the course of 200 kyr (red). Transient ice volume over time from the conceptual model (solid lines) and the PISM results they mimic (dashed lines), for the (b) 100-kyr simulation, (c) 400-kyr simulation, and (d) five times 40-kyr simulation.

$$g(t) = 40 + 120 * \sqrt{\max\left(0, V_{\text{eq\_low}}(C(t)) - V(t) - 9\right)} \, (\text{km}^3/\text{year}) \qquad (4)$$

$$d(t) = 100 + 100 * (V(t) - V_{\text{eq\_top}}(C(t))) \, (\text{km}^3/\text{year}). \qquad (5)$$

The growth and decay rates are dependent on the difference between the ice volume and equilibrium, to simulate the observed increase of the rates when this difference become larger. For the decay rate, we find that this dependence becomes less strong at larger differences in the PISM results, as reflected in the square

Table 3

Conceptual Model Experiments Performed Using the PISM-Derived CO_2-Index-V_{eq} Relation

Name	Forcing period	Forcing amplitude
100kyr	100 kyr	1 (0 to 1)
40kyr	40 kyr	1 (0 to 1)
400kyr	400 kyr	1 (0 to 1)
100kyr_half	100 kyr	0.5 (0.25 to 0.75)
orbit	Based on insolation	1 (0 to 1)
orbit_half	Based on insolation	0.5 (0.25 to 0.75)
orbit_low	Based on insolation	0.5 (0 to 0.5)
orbit_high	Based on insolation	0.5 (0.5 to 1)

Note. Growth and decay rates follow from Equations 4 and 5. Five forcing cycles per experiment are performed for experiments 100kyr, 40kyr, 400kyr, and 100kyr_half. The forcing for experiments orbit, orbit_half, orbit_low, and orbit_high is based on the variability of 80°S January mean insolation (Laskar et al., 2004) over the period 21.5 to 20 Myr ago; only the period 21 to 20 Myr ago is analyzed.

root dependence. Furthermore, a cut-off factor of value 9 is invoked, because otherwise, the decay rate would increase too quickly after a reversal from a growing to a diminishing ice volume. We use the default option of keeping the ice volume unchanged in between the bottom and top branches of the CO_2-index-V_{eq} relation. This simplification does not impede correspondence between the transient conceptual model simulations and the PISM simulations, because this domain is rather small in the equilibrium PISM simulations (see also section 4).

3.2.3. Difference Between Transient and Equilibrium Ice Volume Variability

Our conceptualization explains the main differences between the transient and equilibrium PISM results of Stap et al. (2019) (Figure 5). Using the PISM-derived CO_2-index-V_{eq} relation with these growth and decay rates, we perform experiment 100kyr (Table 3) in which we linearly change the CO_2-index (i) from 1 to 0 to 1 five successive times. Starting from $i = 1$ and zero ice volume, we apply a forcing period of 100 kyr for one CO_2 cycle, so 500 kyr for the complete simulation (Figures 6a and 6b). Because the growth and decay rates are smaller than the equilibrium change rate, we obtain phases of concurrent CO_2 increase (decrease) ice sheet growth (decay), even though the equilibrium ice volume decreases monotonically with CO_2. The onset of ice volume decay trails CO_2 increase by 24.3 kyr or 24% of the forcing period in the equilibrium cycle. Ice volume increase follows 11.0 kyr (11%) after the forcing starts to decrease. The growth phase thus lasts 14.3 kyr longer than the decay phase, as a consequence of the growth rate generally being smaller than the decay rate.

We additionally perform experiments with different forcing periods: 40kyr (Figures 6c and 6d, orange lines) and 400kyr (Figures 6c and 6d, green lines), which show that a lower forcing frequency leads to larger amplitude ice volume variability. The difference between the maximum and minimum ice volumes in the equilibrium cycle increases from 3.2×10^6 km^3 in experiment 40kyr, to 6.2×10^6 km^3 in 100kyr, and 10.1×10^6 km^3 in 400kyr. Meanwhile, the relative phase differences between ice volume and CO_2 are larger in 40kyr: 16% (6.2 kyr) for the onset of the growth phase and 28% (11.1 kyr) for the decay phase. Conversely, with 6% (25.6 kyr) and 20% (78.6 kyr), respectively, the growth and decay phase differences are smaller in 400kyr.

3.2.4. Response to Smaller Forcing Amplitude

Our conceptualization also predicts transient PISM behavior. We here investigate the sensitivity of ice volume to a 50% reduction of the forcing amplitude (Figures 6e and 6f). In experiment 100kyr_half, we cycle the CO_2-index between 0.25 and 0.75. Because the growth rates are generally smaller than the decay rates, this forcing amplitude reduction leads to a slight increase of the equilibrium-cycle mean ice volume from 4.9 to 5.1×10^6 km^3. Meanwhile, the difference between the maximum and minimum ice volumes now reduces by 52% to 3.0×10^6 km^3, most probably as a consequence of the growth and decay rates being dependent on the difference between the ice volume and the equilibrium ice volume. Finally, the phase delays for the growth phase decrease to 10.6 kyr, while it increases to 27.8 kyr for the decay phase. Qualitatively similar results are obtained in the case of 40-kyr and 400-kyr forcing cycles (not shown).

3.3. Response to (Covarying) Miocene Solar Insolation and CO_2 Concentrations

We perform simulations using our conceptual model with the PISM-derived Miocene AIS CO_2-index-V_{eq} relation and CO_2-index forcing based on solar insolation variability. We force the model over the arbitrarily chosen 1.5 million-year time frame from 21.5 to 20 Myr ago and use only the final million years simulated (21 to 20 Myr ago) for our analysis. We vary the CO_2-index forcing, in sync with the 80°S January mean insolation curve (Laskar et al., 2004) (Figure 1, blue), between 0 and 1 (experiment orbit, Table 3). Mind that solar insolation itself is not included in the PISM results underlying the conceptual model setup.

The resulting ice volume exhibits an asymmetric, sawtooth response to the forcing (Figure 7a), as is also observed in benthic δ^{18}O records (Liebrand et al., 2017). The ice volume furthermore shows no clear relation to the forcing CO_2-index (Figure 7b), in contrast to the equilibrium ice volume. This is due to the intertwined
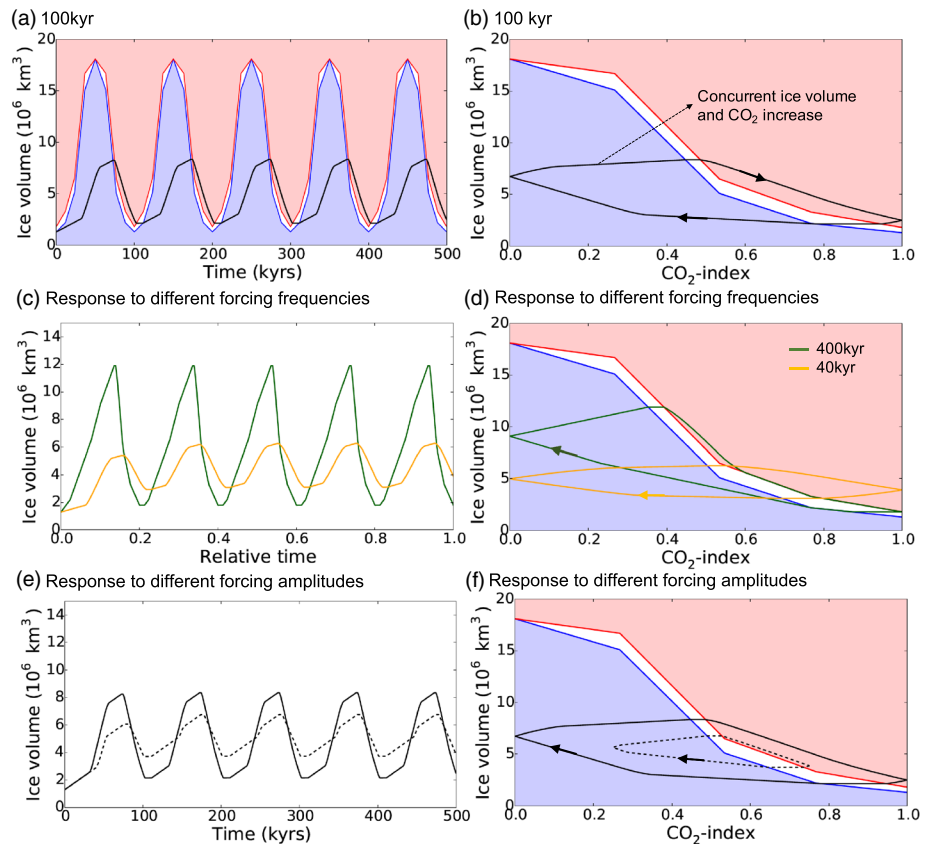
Figure 6. Results of the conceptual model using the PISM-derived CO_2-index-V_{eq} relation (Figure 2b). Black lines show the (a) evolution of ice volume over time and (b) equilibrium-cycle relation between the CO_2-index and ice volume, for experiment 100kyr. (c, d) Similar for experiments 40kyr (orange) and 400kyr (green) (in panel c, relative time is shown). (e, f) Similar for experiments 100kyr (solid) and 100kyr_half (dashed).

frequencies with different, time-varying strengths comprising the forcing signal. The amplitude of ice volume variability is suppressed as a consequence of the dominant precession component in the forcing, which grants only short periods of growth to the ice sheet. Generally, ice volume follows the precession cycles, but some are skipped. This can happen when eccentricity decreases from one precession cycle to the next, and consequently, the amplitude of precession variability becomes smaller.

Similar to our findings in section 3.2, decreasing the amplitude of CO_2-index variations from 1 to 0.5—now varying it between 0.25 and 0.75 (experiment orbit_half)—leads to a 7% larger mean ice volume of 5.92 compared to 5.52×10^6 km^3 (not shown). Similar features have been described for the influence of temperature variability on future Greenland (Mikkelsen et al., 2018) and Pleistocene Northern Hemisphere ice sheet evolution (Abe-Ouchi et al., 2013; Niu et al., 2019). We perform two more simulations with the CO_2-index covarying with insolation between 0 and 0.5 (orbit_low; Figure 7d, orange lines) and between 0.5 and 1 (orbit_high; Figures 7c and 7d, green lines). In orbit_high, the ice volume remains very small throughout the entire simulated period. For the CO_2 range in orbit_low, however, the CO_2-index-V_{eq} relation is much steeper. This causes higher growth rates and consequently larger amplitude ice volume variability, because of the increased differences between ice volume and equilibrium ice volume. Particularly toward eccentricity minima, the ice volume grows substantially, hence constituting a 400-kyr eccentricity cycle, similar to the one observed in the stacked benthic δ^{18}O record of Zachos et al. (2008) (Figure 1, red).

These simulations show how the delayed and nonlinear response of the AIS to (covarying) solar insolation and CO_2 concentrations alone can already modulate power in the benthic δ^{18}O spectrum. Moreover, they corroborate a significant effect of the mean CO_2 and amplitude of CO_2 variability, on the relation between insolation and ice volume (Figures 7e and 7f) and hence benthic δ^{18}O during the Miocene (Holbourn et al., 2005, 2013, 2015, 2018).
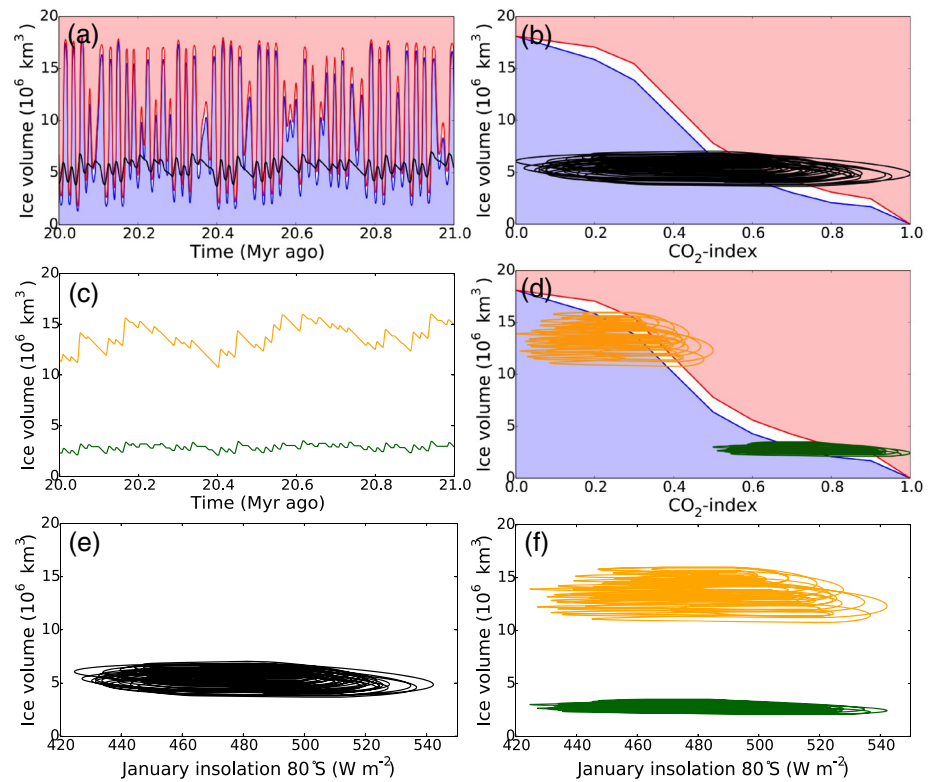
Figure 7. Results of the conceptual model using the PISM-derived CO_2-index-V_{eq} relation (Figure 2b). Black lines show the (a) evolution of ice volume over the period 21 to 20 Myr ago and (b) relation between the CO_2-index and ice volume, for experiment orbit. (c, d) Similar for experiments orbit_low (orange) and orbit_high (green). (e, f) Relation between 80°S January mean insolation (Laskar et al., 2004) and ice volume, for the same experiments.

4. Discussion

Discrepancies between Southern Hemisphere solar insolation and benthic $\delta^{18}O$ variability during the Miocene can be caused by the influence of deep-sea temperature changes and by CO_2 (and other greenhouse gas) concentrations not covarying with solar insolation. In section 3.3, we have shown that these discrepancies can also result from the delayed and nonlinear response of Antarctic ice volume to (covarying) solar insolation and CO_2 concentrations. In reality, however, CO_2 concentration changes do not simply follow insolation variability even on orbital timescales and can have counterbalancing effects on the AIS. In fact, AIS changes can affect the carbon cycle (Wadham et al., 2019), for example, by their effect on chemical weathering (Lear et al., 2004; Shevenell et al., 2008) and organic carbon burial rates (Badger et al., 2013; Kump & Arthur, 1999; Sosdian et al., 2020), as is reflected in benthic $\delta^{13}C$ records. In the future, the carbon cycle should therefore be integrated in both the physically based setup (Ganopolski & Brovkin, 2017) and in the conceptual model (Paillard & Parrenin, 2004), to additionally capture interactions between ice sheets, the climate, and the carbon cycle.

Furthermore, the PISM results underlying our conceptual model setup do not include the effects of orbital variability, and they are climatically forced offline. Consequently, important climate-ice sheet feedbacks, such as the albedo-temperature feedback, are neglected (e.g., DeConto & Pollard, 2003; Gasson et al., 2016; Gregory et al., 2012; Herrington & Poulsen, 2011; Ladant et al., 2014; Stap et al., 2014; Tan et al., 2018; Verbitsky et al., 2018). In addition, GCM modeling has shown large model dependencies on the AIS temperature forcing at different CO_2 levels, stemming from the implemented physics (e.g., Gasson et al., 2014; Lunt et al., 2012). Hence, in reality, the range of CO_2 levels where significant AIS changes occur is most likely different from what the PISM simulations we have used here suggest. We have accounted for this by normalizing the CO_2 changes using an index. Moreover, hysteresis in the CO_2-index-V_{eq} relation might be larger (e.g., Gasson et al., 2016). Our analysis in Appendix A shows that increased hysteresis does not qualitatively affect our main results. However, how to conceptually model ice sheet changes in between the

bottom and top branches of the CO_2-index-V_{eq} relation remains elusive. Keeping the ice volume unchanged in between the bottom and top branches suffices to obtain reasonably close correspondence between the transient conceptual model simulations and the PISM simulations of Stap et al. (2019). With increased hysteresis, however, this will likely not be the case, necessitating a comprehensive investigation of equilibrium (coupled climate and) ice volume simulations started from "in between" initial CO_2 and ice volume states.

Lastly, inclusion of climate-ice sheet feedbacks can also affect the pace of ice volume changes and therefore the difference between the growth and decay rates and the equilibrium ice volume change rates of the Miocene AIS. Hence, our results should be re-evaluated quantitatively, once a sufficient number of equilibrium simulations from coupled ice sheet-climate models including orbital variability are available to serve as a basis for our conceptual model setup.

5. Conclusions

Usually, concurrent ice volume increase and CO_2 level rise are explained as a consequence of increased precipitation outweighing increased surface melt in a warmer climate (Oerlemans, 1991). This reasoning only needs to consider ice sheets in equilibrium with the forcing climate. However, here we have explored how it is possible to obtain ice volume growth during CO_2 increase without the necessity for this characteristic of the equilibrium mass balance. We have deployed a conceptual model in the vein of earlier models of transient ice volume variability (e.g., Calder, 1974; Huybers, 2009; Huybers & Wunsch, 2005; Imbrie & Imbrie, 1980; Parrenin & Paillard, 2003), to analyze the difference in tendency between the transient ice volume variability and equilibrium differences.

Our main finding is that in our simulations, the ice sheet continues to adapt to a relatively large equilibrium ice sheet after a CO_2 decrease, when the CO_2 level is already increasing again. This is purely a consequence of the disequilibrium of the ice sheet, the growth rate being smaller than the change rate of the equilibrium ice volume, in combination with the transient forcing. We have used Southern Hemisphere insolation variability as a basis for CO_2-index forcing over the period 21 to 20 Myr ago. Our results indicate that the delayed and nonlinear response of the AIS to (covarying) solar insolation and CO_2 concentrations can lead to "skipped" forcing cycles and modulation of power in the benthic $\delta^{18}O$ spectrum. Hence, we conclude that this response is in part the cause of discrepancies between Southern Hemisphere solar insolation and benthic $\delta^{18}O$ variability during the Miocene.

We have further found that higher frequency CO_2 variability increases the relative phase lag between ice volume and CO_2/temperature. Furthermore, because the growth rates are smaller than the decay rates of the Miocene AIS, the growth phase lasts longer than the decay phase under symmetrical forcing. Finally, the amplitude of CO_2 variability influences the mean ice volume, as a consequence of the growth rates being smaller than the decay rates. Decreased CO_2 variability also leads to a smaller amplitude of ice volume variability, because the growth and decay rates are not constant but depend on the forcing.

In light of our results, not only the value of CO_2 concentrations but also an accurate timing of their tendency is very important to constrain ice modeling studies. In particular, the phase relation with benthic $\delta^{18}O$ variations is of great interest. This calls for the retrieval of high temporal resolution proxy-CO_2 and benthic $\delta^{18}O$ records with good age control, over at least parts of the early and mid-Miocene.

Appendix A: Influence of Hysteresis

We repeat our experiments $g_{0.002}d_{0.004}$ and $g_{0.002}d_{0.004}$_half of section 3.1 and perform a new simulation using a reduced period of 100 time steps instead of 200. We now implement a piecewise linear C-V_{eq} relation with appreciable hysteresis. The top branch solution drops from 1 to 0.7 for $0 \leq C \leq 0.5$ and then from 0.7 to 0 for $0.5 \leq C \leq 1$. The bottom branch solution drops from 1 to 0.3 for $0 \leq C \leq 0.5$ and then from 0.3 to 0 for $0.5 \leq C \leq 1$. We handle the situation when an ice sheet has a volume in between the bottom and top branch equilibrium ice volume in three different ways: (1) keeping the ice volume unchanged (our default option), (2) letting it grow by the specified growth rate, and (3) letting it decay by the specified decay rate. Qualitatively, most of our main results remain unaffected. In fact, Case 2 yields the same results as simply implementing only the top branch equilibrium solution without hysteresis and likewise Case 3 as the bottom branch solution. We observe phases of concurrent ice sheet growth (decay) under rising (falling) C
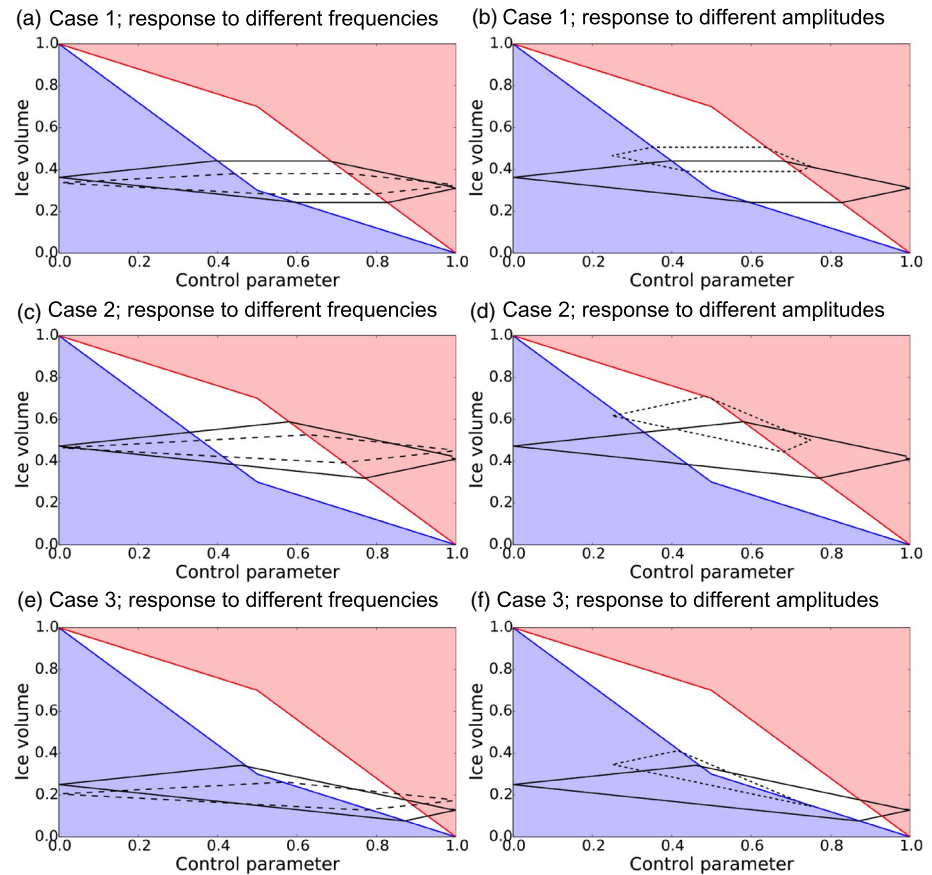
Figure A1. Results of the conceptual model using a piecewise linear C-V_{eq} relation with appreciable hysteresis. Equilibrium-cycle relation between the control parameter and ice volume for our reference experiment (solid lines), decreased forcing frequency (long dashed lines), and decreased forcing amplitude (dashed lines). Results for different ways of handling the situation when an ice sheet has a volume in between the bottom and top branch equilibrium ice volume: (a, b) Case 1, keeping the ice volume unchanged; (c, d) Case 2, letting it grow; and (e, f) Case 3, letting it decay.

in all investigated cases, although the duration of these phases differs among the cases. In all cases, these phases last relatively longer with increased forcing frequency (Figure A1, solid and long dashed lines). Furthermore, the ratio between the growing and decaying phases and hence the amplitude of ice volume variability differs among the cases, but the phases of ice sheet growth always last longer than that of ice sheet decay in the equilibrium cycle. Lastly, a reduced amplitude forcing variability leads to an increase of the mean ice volume (Figure A1, solid and dashed lines). Other than before, however, the amplitude of ice volume variability is reduced when the ice sheet is kept unchanged when its volume is in between the bottom and top branch equilibrium ice volume (Figure A1b). In the other cases, ice volume variability remains unaffected (Figures A1d and A1f).

Data Availability Statement

The data from the conceptual model simulations presented in this paper (https://doi.pangaea.de/10.1594/PANGAEA.907521) and the code of the conceptual model (https://github.com/lbstap/Comics) are available and can be retrieved online.

References

Abe-Ouchi, A., Saito, F., Kawamura, K., Raymo, M. E., Okuno, J., Takahashi, K., & Blatter, H. (2013). Insolation-driven 100,000-year glacial cycles and hysteresis of ice-sheet volume. *Nature*, *500*(7461), 190.

Badger, M. P. S., Lear, C. H., Pancost, R. D., Foster, G. L., Bailey, T. R., Leng, M. J., & Abels, H. A. (2013). CO_2 drawdown following the middle Miocene expansion of the Antarctic ice sheet. *Paleoceanography*, *28*, 42–53. https://doi.org/10.1002/palo.20015

Bijl, P. K., Houben, A. J. P., Hartman, J. D., Pross, J., Salabarnada, A., Escutia, C., & Sangiorgi, F. (2018). Paleoceanography and ice sheet variability offshore Wilkes Land, Antarctica—Part 2: Insights from Oligocene-Miocene dinoflagellate cyst assemblages. *Climate of the Past*, *14*(7), 1015–1033.

Billups, K., & Schrag, D. P. (2002). Paleotemperatures and ice volume of the past 27 Myr revisited with paired Mg/Ca and 18O/16O measurements on benthic foraminifera. *Paleoceanography*, *17*(1), 1–11. https://doi.org/10.1029/2000PA000567

Bueler, E., & Brown, J. (2009). Shallow shelf approximation as a "sliding law" in a thermodynamically coupled ice sheet model. *Journal of Geophysical Research*, *114*, F03008. https://doi.org/10.1029/2008JF001179

Calder, N. (1974). Arithmetic of ice ages. *Nature*, *252*(5480), 216–218.

Colleoni, F., De Santis, L., Montoli, E., Olivo, E., Sorlien, C. C., Bart, P. J., et al. (2018). Past continental shelf evolution increased Antarctic ice sheet sensitivity to climatic conditions. *Scientific Reports*, *8*(1), 11323.

Cramer, B. S., Toggweiler, J. R., Wright, J. D., Katz, M. E., & Miller, K. G. (2009). Ocean overturning since the Late Cretaceous: Inferences from a new benthic foraminiferal isotope compilation. *Paleoceanography*, *24*, PA4216. https://doi.org/10.1029/2008PA001683

De Vleeschouwer, D., Vahlenkamp, M., Crucifix, M., & Pälike, H. (2017). Alternating Southern and Northern Hemisphere climate response to astronomical forcing during the past 35 m.y. *Geology*, *45*(4), 375–378.

DeConto, R. M., & Pollard, D. (2003). Rapid Cenozoic glaciation of Antarctica induced by declining atmospheric CO_2. *Nature*, *421*(6920), 245.

Fretwell, P., Pritchard, H. D., Vaughan, D. G., Bamber, J. L., Barrand, N. E., Bell, R., et al. (2013). Bedmap2: Improved ice bed, surface and thickness datasets for Antarctica. *The Cryosphere*, *7*(1), 375–393.

Ganopolski, A., & Brovkin, V. (2017). Simulation of climate, ice sheets and CO_2 evolution during the last four glacial cycles with an Earth system model of intermediate complexity. *Climate of the Past*, *13*, 1695–1716.

Gasson, E., DeConto, R. M., Pollard, D., & Levy, R. H. (2016). Dynamic Antarctic ice sheet during the early to mid-Miocene. *Proceedings of the National Academy of Sciences*, *113*(13), 3459–3464.

Gasson, E., Lunt, D. J., DeConto, R., Goldner, A., Heinemann, M., Huber, M., et al. (2014). Uncertainties in the modelled CO_2 threshold for Antarctic glaciation. *Climate of the Past*, *10*(2), 451–466.

Gregory, J. M., Browne, O. J. H., Payne, A. J., Ridley, J. K., & Rutt, I. C. (2012). Modelling large-scale ice-sheet–climate interactions following glacial inception. *Climate of the Past*, *8*(5), 1565–1580.

Hartman, J. D., Sangiorgi, F., Salabarnada, A., Peterse, F., Houben, A. J. P., Schouten, S., et al. (2018). Paleoceanography and ice sheet variability offshore Wilkes Land, Antarctica—Part 3: Insights from Oligocene–Miocene TEX_{86}-based sea surface temperature reconstructions. *Climate of the Past*, *14*(9), 1275–1297.

Herrington, A. R., & Poulsen, C. J. (2011). Terminating the Last Interglacial: The role of ice sheet–climate feedbacks in a GCM asynchronously coupled to an ice sheet model. *Journal of Climate*, *25*(6), 1871–1882.

Holbourn, A. E., Kuhnt, W., Clemens, S. C., Kochhann, K. G. D., Jöhnck, J., Lübbers, J., & Andersen, N. (2018). Late Miocene climate cooling and intensification of southeast Asian winter monsoon. *Nature Communications*, *9*(1), 1–13.

Holbourn, A. E., Kuhnt, W., Clemens, S., Prell, W., & Andersen, N. (2013). Middle to late Miocene stepwise climate cooling: Evidence from a high-resolution deep water isotope curve spanning 8 million years. *Paleoceanography*, *28*, 688–699. https://doi.org/10.1002/2013PA002538

Holbourn, A. E., Kuhnt, W., Kochhann, K. G. D., Andersen, N., & Sebastian Meier, K. J. (2015). Global perturbation of the carbon cycle at the onset of the Miocene Climatic Optimum. *Geology*, *43*(2), 123–126.

Holbourn, A. E., Kuhnt, W., Schulz, M., & Erlenkeuser, H. (2005). Impacts of orbital forcing and atmospheric carbon dioxide on Miocene ice-sheet expansion. *Nature*, *438*(7067), 483–487.

Hutchinson, D. K., Coxall, H. K., O'Regan, M., Nilsson, J., Caballero, R., & de Boer, A. M. (2019). Arctic closure as a trigger for Atlantic overturning at the Eocene-Oligocene Transition. *Nature Communications*, *10*(1), 1–9.

Huybers, P. (2009). Pleistocene glacial variability as a chaotic response to obliquity forcing. *Climate of the Past*, *5*(3), 481–488. https://doi.org/10.5194/cp-5-481-2009

Huybers, P., & Wunsch, C. (2005). Obliquity pacing of the late Pleistocene glacial terminations. *Nature*, *434*(7032), 491.

Imbrie, J., & Imbrie, J. Z. (1980). Modeling the climatic response to orbital variations. *Science*, *207*(4434), 943–953.

John, C. M., Karner, G. D., Browning, E., Leckie, R. M., Mateo, Z., Carson, B., & Lowery, C. (2011). Timing and magnitude of Miocene eustasy derived from the mixed siliciclastic-carbonate stratigraphic record of the northeastern Australian margin. *Earth and Planetary Science Letters*, *304*(3–4), 455–467.

Jungclaus, J. H., Keenlyside, N., Botzet, M., Haak, H., Luo, J.-J., Latif, M., et al. (2006). Ocean circulation and tropical variability in the coupled model ECHAM5/MPI-OM. *Journal of Climate*, *19*(16), 3952–3972.

Kominz, M. A., Browning, J. V., Miller, K. G., Sugarman, P. J., Mizintseva, S., & Scotese, C. R. (2008). Late Cretaceous to Miocene sea-level estimates from the New Jersey and Delaware coastal plain coreholes: An error analysis. *Basin Research*, *20*(2), 211–226.

Kump, L. R., & Arthur, M. A. (1999). Interpreting carbon-isotope excursions: Carbonates and organic matter. *Chemical Geology*, *161*(1–3), 181–198.

Ladant, J.-B., Donnadieu, Y., Lefebvre, V., & Dumas, C. (2014). The respective role of atmospheric carbon dioxide and orbital parameters on ice sheet evolution at the Eocene-Oligocene transition. *Paleoceanography*, *29*, 810–823. https://doi.org/10.1002/2013PA002593

Langebroek, P. M., Paul, A., & Schulz, M. (2010). Simulating the sea level imprint on marine oxygen isotope records during the middle Miocene using an ice sheet–climate model. *Paleoceanography*, *25*, PA4203. https://doi.org/10.1029/2008PA001704

Laskar, J., Robutel, P., Joutel, F., Gastineau, M., Correia, A. C. M., & Levrard, B. (2004). A long-term numerical solution for the insolation quantities of the Earth. *Astronomy & Astrophysics*, *428*(1), 261–285. https://doi.org/10.1051/0004-6361:20041335

Lear, C. H., Mawbey, E. M., & Rosenthal, Y. (2010). Cenozoic benthic foraminiferal Mg/Ca and Li/Ca records: Toward unlocking temperatures and saturation states. *Paleoceanography*, *25*, PA4215. https://doi.org/10.1029/2009PA001880

Lear, C. H., Rosenthal, Y., Coxall, H. K., & Wilson, P. A. (2004). Late Eocene to early Miocene ice sheet dynamics and the global carbon cycle. *Paleoceanography*, *19*, PA4015. https://doi.org/10.1029/2004PA001039

Levy, R. H., Harwood, D., Florindo, F., Sangiorgi, F., Tripati, R., Von Eynatten, H., et al. (2016). Antarctic ice sheet sensitivity to atmospheric CO_2 variations in the early to mid-Miocene. *Proceedings of the National Academy of Sciences*, *113*(13), 3453–3458.

Levy, R. H., Meyers, S. R., Naish, T. R., Golledge, N. R., McKay, R. M., Crampton, J. S., et al. (2019). Antarctic ice-sheet sensitivity to obliquity forcing enhanced through ocean connections. *Nature Geoscience*, *12*, 132–137.

Liebrand, D., de Bakker, A. T. M., Beddow, H. M., Wilson, P. A., Bohaty, S. M., Ruessink, G., et al. (2017). Evolution of the early Antarctic ice ages. *Proceedings of the National Academy of Sciences*, *114*, 3867–3872.

Liebrand, D., Lourens, L. J., Hodell, D. A., de Boer, B., van de Wal, R. S. W., & Pälike, H. (2011). Antarctic ice sheet and oceanographic response to eccentricity forcing during the early Miocene. *Climate of the Past*, *7*(3), 869–880.

Locarnini, R. A., Mishonov, A. V., Antonov, J. I., Boyer, T. P., Garcia, H. E., Baranova, O. K., et al. (2010). World ocean atlas 2009, vol. 1, temperature. In S. Levitus (ed.), *NOAA Atlas NESDIS 66* (pp. 184). Washington, DC: US Gov. Printing Office.

Lunt, D. J., Dunkley Jones, T., Heinemann, M., Huber, M., LeGrande, A., Winguth, A., et al. (2012). A model–data comparison for a multi-model ensemble of early Eocene atmosphere–ocean simulations: EoMIP. *Climate of the Past*, *8*, 1717–1736.

Maslin, M. A., Li, X. S., Loutre, M.-F., & Berger, A. (1998). The contribution of orbital forcing to the progressive intensification of Northern Hemisphere glaciation. *Quaternary Science Reviews*, *17*(4–5), 411–426.

Mikkelsen, T. B., Grinsted, A., & Ditlevsen, P. (2018). Influence of temperature fluctuations on equilibrium ice sheet volume. *The Cryosphere*, *12*(1), 39–47.

Miller, K. G., Kominz, M. A., Browning, J. V., Wright, J. D., Mountain, G. S., Katz, M. E., et al. (2005). The Phanerozoic record of global sea-level change. *Science*, *310*(5752), 1293–1298.

Niu, L., Lohmann, G., & Gowan, E. J. (2019). Climate noise influences ice sheet mean state. *Geophysical Research Letters*, *46*, 9690–9699. https://doi.org/10.1029/2019GL083717

Oerlemans, J. (1991). The role of ice sheets in the Pleistocene climate. *Norsk Geologisk Tidsskrift*, *71*, 155–161.

Paillard, D., & Parrenin, F. (2004). The Antarctic ice sheet and the triggering of deglaciations. *Earth and Planetary Science Letters*, *227*(3–4), 263–271.

Parrenin, F., & Paillard, D. (2003). Amplitude and phase of glacial cycles from a conceptual model. *Earth and Planetary Science Letters*, *214*(1–2), 243–250.

Shevenell, A. E., Kennett, J. P., & Lea, D. W. (2008). Middle Miocene ice sheet dynamics, deep-sea temperatures, and carbon cycling: A Southern Ocean perspective. *Geochemistry, Geophysics, Geosystems*, *9*, Q02006. https://doi.org/10.1029/2007GC001736

Sosdian, S. M., Babila, T. L., Greenop, R., Foster, G. L., & Lear, C. H. (2020). Ocean carbon storage across the middle Miocene: a new interpretation for the Monterey Event. *Nature Communications*, *11*(1), 1–11.

Stärz, M., Jokat, W., Knorr, G., & Lohmann, G. (2017). Threshold in North Atlantic-Arctic Ocean circulation controlled by the subsidence of the Greenland-Scotland Ridge. *Nature Communications*, *8*, 15681. https://doi.org/10.1038/ncomms15681

Stap, L. B., Sutter, J., Knorr, G., Stärz, M., & Lohmann, G. (2019). Transient variability of the Miocene Antarctic ice sheet smaller than equilibrium differences. *Geophysical Research Letters*, *46*, 4288–4298. https://doi.org/10.1029/2019GL082163

Stap, L. B., van de Wal, R. S. W., De Boer, B., Bintanja, R., & Lourens, L. J. (2014). Interaction of ice sheets and climate during the past 800 000 years. *Climate of the Past*, *10*(6), 2135–2152.

Tan, N., Ladant, J.-B., Ramstein, G., Dumas, C., Bachem, P., & Jansen, E. (2018). Dynamic Greenland ice sheet driven by pCO_2 variations across the Pliocene Pleistocene transition. *Nature Communications*, *9*(1), 1–9.

Uppala, S. M., Kållberg, P. W., Simmons, A. J., Andrae, U., Bechtold, V., Fiorino, M., et al. (2005). The ERA-40 re-analysis. *Quarterly Journal of the Royal Meteorological Society*, *131*(612), 2961–3012.

Verbitsky, M. Y., Crucifix, M., & Volobuev, D. M. (2018). A theory of Pleistocene glacial rhythmicity. *Earth System Dynamics*, *9*(3), 1025–1043.

Wadham, J. L., Hawkings, J. R., Tarasov, L., Gregoire, L. J., Spencer, R. G. M., Gutjahr, M., et al. (2019). Ice sheets matter for the global carbon cycle. *Nature Communications*, *10*(1), 1–17.

Weertman, J. (1964). The theory of glacier sliding. *Journal of Glaciology*, *5*(39), 287–303.

Winkelmann, R., Martin, M. A., Haseloff, M., Albrecht, T., Bueler, E., Khroulev, C., & Levermann, A. (2011). The Potsdam Parallel Ice Sheet Model (PISM-PIK) Part 1: Model description. *The Cryosphere*, *5*, 715–726.

Zachos, J. C., Dickens, G. R., & Zeebe, R. E. (2008). An early Cenozoic perspective on greenhouse warming and carbon-cycle dynamics. *Nature*, *451*(7176), 279–283.